Comparison study of algorithms and accuracy in the wavelength scanning interferometry

Hussam Muhamedsalih, Feng Gao, and Xiangqian Jiang*

Centre for Precision Technologies, University of Huddersfield, Huddersfield HD1 3DH, UK

*Corresponding author: x.jiang@hud.ac.uk

Received 8 August 2012; revised 6 October 2012; accepted 28 November 2012;
posted 29 November 2012 (Doc. ID 174048); published 20 December 2012

Wavelength scanning interferometry (WSI) can be used for surface measurement with discontinuous surface profiles by producing phase shifts without any mechanical scanning process. The choice of algorithms for the WSI to analyze the fringe pattern depends on the desired accuracy and computing speed. This paper provides comparison of four different algorithms to analyze the interference fringe pattern acquired from WSI. The mathematical description of these algorithms, their computing resolution, and speed are presented. Two step-height samples are measured using the WSI. Experimental results demonstrate that the accuracy of measuring surface height varies from micrometer to nanometer value depending on the algorithm used to analyze the captured interferograms. © 2012 Optical Society of America

OCIS codes: 120.0120, 120.2650.

1. Introduction

Modern manufacturing processes can produce surface textures and structures ranging from submillimeter to nanometer value, such as surfaces produced by milling machines and photo etching process. This wide range demands a variety of instruments to assess the manufactured surface. For micro/nanoscale surface textures, interferometry is widely used for measurement. Examples of interferometer techniques are phase shifting interferometry (PSI), scanning white light interferometry (SWLI), and wavelength scanning interferometry (WSI) [1–4]. The PSI is typically limited to measurements of nanoscale surface texture. This limitation can be overcome by using SWLI. The measurement speed of SWLI, however, is relatively slow due to the mechanical scanning. WSI can be employed to measure absolute distances without the 2π phase ambiguity limitation of PSI and in a shorter time than SWLI. The key principle of this interferometry WSI is to shift the phase of the interfered beams by scanning the wavelength instead of altering the optical path difference mechanically. This has the advantage of overcoming limits due to the mechanical dynamics, such as hysteresis and nonlinearity, which are inherent in any mechanical scanning method.

In early implementations of WSI, the wavelength was tuned over a range of several nanometers using tuning laser diodes. This narrow scanning range and the mode hopping problems that exist in laser diodes limited the measurement accuracy to submillimeter [5,6]. However, this limitation was overcome by combining the WSI using external cavity laser diodes with other high precision interferometry techniques, such as heterodyne, to achieve nanometer accuracy [7,8].

Measurement resolution in the WSI was then further improved by increasing the wavelength scanning range. A scanning range up to 100 nm was achieved by using either a solid state laser, such as Ti:sapphire [9], or an acousto-optic tunable filter (AOTF) coupled to a halogen light source [10]. Further enhancement in the measurement resolution made clear that the selection of a suitable algorithm could achieve nanometer accuracy without the need to combine WSI with other interferometry techniques.

1559-128X/12/368854-09$15.00/0

The Fourier transform is used commonly to analyze periodic interference patterns and acquire the phase. In general, the fast Fourier transform (FFT) is used to compute the power spectral density of the interference pattern. The interference pattern also can be analyzed by using convolution to determine the period of the interference cycles.

This paper discussed four algorithms that analyze interferometric data acquired from a WSI instrument. Two algorithms are based on finding the amount of phase shift directly from the power spectral density of the interference pattern using a discrete Fourier transform. The other two algorithms are based on analyzing the interference pattern to find the phase shift slope using the discrete Fourier transform and locating the peaks of the pattern with respect to the scanning wavelength range.

2. Principle

The basic configuration of the WSI used in this paper is illustrated in Fig. 1. The wavelength scanning process is achieved by using an AOTF to filter a narrow band from a halogen light source. The filtered wavelength can be scanned over a wide range with a high speed. The fast AOTF scanning rate made the overall acquisition time to be limited by the CCD speed only.

The central wavelength of light that diffracted by the AOTF can be determined by the equation [11]

$$\lambda = \alpha \Delta n \frac{v_a}{f_a}, \tag{1}$$

where α is a constant that depends on the incident angle of entrance light beam, Δn is the birefringence crystal refractive index, and ν_a and f_a are the propagation velocity and frequency of the applied acoustic wave, respectively.

Equation (1) shows that the filtered wavelength depends on the acoustic wave frequency (AOTF driving frequency). Thus, when the frequency is driven in a linear manner, the reciprocal of the wavelength can be scanned linearly; Δn may be assumed to be a constant at the applied frequency. Therefore this scanning process can provide a linear phase shift for the interference pattern. In this experiment, the filtered wavelength is scanned from 683.42 to 590.29 nm ranges. The obtained spectral linewidth of the filtered light is dependent on the tuned wavelength and ranges from 1.7 to 2 nm at FWHM. This linewidth scale can provide a coherence length up to 96 μm. The filtered wavelength is scanned in 0.36 nm increments. At each increment step, a single frame is captured with 640 × 480 pixels with 256 frames captured through the entire scanning wavelength range. The overall capture time is approximately 2.6 s. Each captured frame has a unique wavelength, with each frame pixel representing a specific point on the measured surface. By considering a single pixel across all captured frames, a periodic sinusoidal intensity distribution is obtained for a single point on the measured surface (see Fig. 2). Equation (2) is a mathematical representation of the intensity distribution,

$$I_{xy}(\lambda) = a_{xy}(\lambda) + b_{xy}(\lambda)\cos(\phi_{xy}(\lambda)), \tag{2}$$

whereas $a_{xy}(\lambda)$ and $b_{xy}(\lambda)$ are the background intensity and fringe visibility, respectively, and λ is the scanned wavelength. The x and y indices are the pixel number in the horizontal and vertical directions of the area CCD detector, respectively.

The phase shift of the interference pattern owing to the wavelength shift, $\Delta\varphi_{xy}(\lambda)$, is given by

$$\Delta\varphi_{xy}(\lambda) = \frac{4\pi}{\lambda_s} h_{xy}, \tag{3}$$

where h_{xy} is the sample surface and the λ_s is the synthetic wavelength that is defined by

$$\lambda_s = \frac{\lambda_{\max}\lambda_{\min}}{\lambda_{\max} - \lambda_{\min}}. \tag{4}$$

The synthetic wavelength for the given range is 4.331 μm. The h_{xy} in Eq. (5) is related to half of

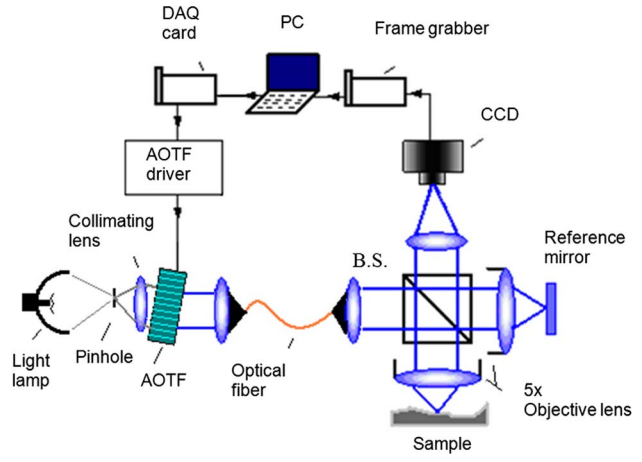

Fig. 1. (Color online) Schematic drawing of a wavelength scanning surface measurement system. AOTF, acousto-optic tunable filter; DAQ, data acquisition card; BS, beam-splitter; and PC, personal computer.

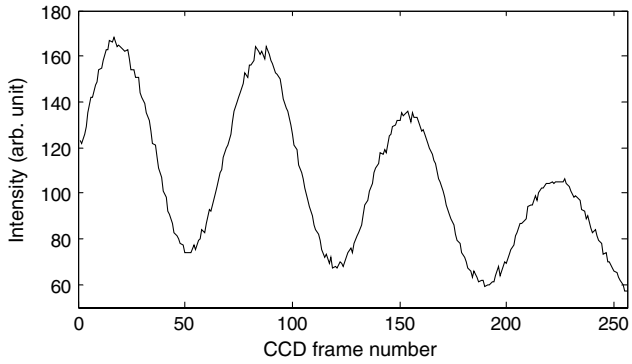

Fig. 2. Interference pattern obtained from a single pixel.

the total optical path difference in the interferometer and can therefore be obtained by determining the absolute of the phase change through the entire wavelength scanning range, as shown in Eq. (5):

$$h_{xy} = \frac{\Delta\varphi\lambda_s}{4\pi}. \tag{5}$$

Various algorithms may be used to determine the phase change relating to the surface height of the measured surface. The following section describes the resolution of the measurement for four different algorithms. This description assumed that the number of captured data causes no oversampling when representing the interference pattern.

3. Analysis of Phase Determining Algorithms

The resolution of surface height measurement using WSI is varied depending on the algorithms that are used to evaluate the phase obtained from the source wavelength scanning process operation. With more accurate determination of the phase shift, higher resolution can be obtained. There have been several computing algorithms proposed previously to determine the amount of phase shift [12–15]. This paper discusses four algorithms and uses them to analyze real measurement data acquired from the WSI described in Section 2. The first algorithm uses FFT to determine the power spectral density of the interference pattern. The phase shift is determined by identifying the fundamental frequency (number of the interference cycle per wavelength scanning range) from the power spectrum. The second algorithm uses a fitted spectrum to estimate the frequency more accurately, thus increasing the resolution. The third algorithm uses an FFT to analyze the sinusoidal interference pattern and isolate the phase information from other unwanted data, such as the DC component and the conjugate term of the phase. Finally, the fourth algorithm identifies the peak positions of the sinusoidal interference pattern with respect to the scanned wavelength range.

A. Phase Shift Determination Using Simple FFT: Algorithm A

Phase shift determination using this method is based on determining the number of cycles of the sinusoidal interference pattern. The number of cycles is determined directly from identifying the Fourier peak of the spectrum, as shown in Fig. 3. Since each cycle represents a 2π phase shift, the overall phase shift can be calculated by multiplying the number of cycles by 2π. The surface height may then be calculated using Eq. (5). The main drawback of this method is that the determination of phase shift is limited to a 2π phase interval, which limits the surface height resolution to the micrometer scale. The resolution can be calculated by the given equation:

$$\delta h = \frac{\delta\varphi\lambda_s}{4\pi}, \tag{6}$$

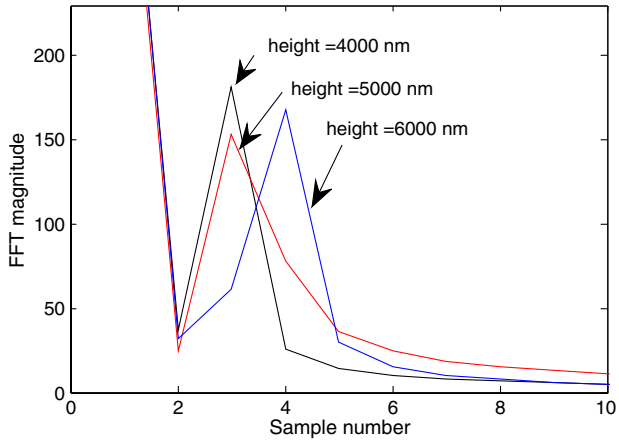

Fig. 3. (Color online) Fourier power spectral density for different heights.

where δh and $\delta\varphi$ are the resolutions of the surface height and phase, respectively. $\delta\varphi$ is equal to 2π for this algorithm. This yields Eq. (6) to be

$$\delta h = \frac{\lambda_s}{2}. \tag{7}$$

Thus the height resolution for the given synthetic wavelength in this paper is 2.165 μm.

B. Phase Shift Determination Using Fitted FFT: Algorithm B

Yamamoto *et al.* used a fitted spectrum to determine the phase shift. The surface height resolution is improved to submicrometer by using a parabolic fitting onto three data points around the Fourier peak [12]. The general formula of a parabola is given by equation

$$f(x) = ax^2 + bx + c, \tag{8}$$

where a, b, and c are the parameters of the quadratic equation. Least squares quadratic polynomial approximation and Gauss elimination can be used to fit the data (see Fig. 4) and determine the equation's parameters (i.e., a, b, and c). Since the slope at the peak of curve is equal to zero, the Fourier peak position can be calculated from the first derivative of Eq. (8), as given in equation

$$x = -b/(2a). \tag{9}$$

This method is able to detect phase variations of less than 2π. The estimated Fourier peak position is multiplied by 2π and is taken as the phase shift value in Eq. (5) in order to calculate the surface height.

C. Interference Pattern Analysis Using Fourier Transform: Algorithm C

The resolution of WSI can be much improved by determining the optical path difference from the slope of the phase shift. The phase shift determination

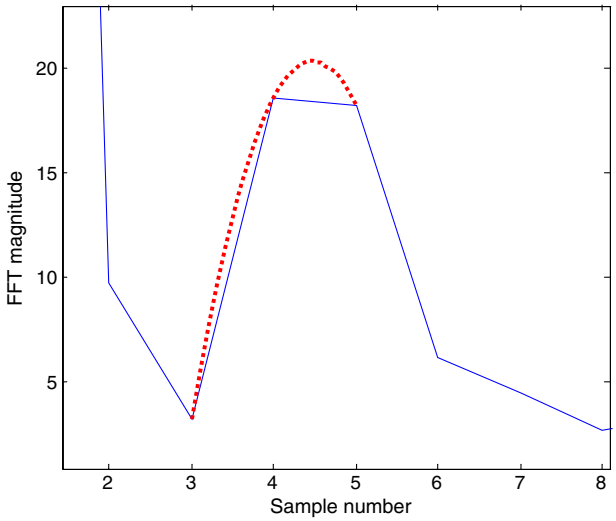

Fig. 4. (Color online) Fourier power spectral density for 7490 nm single point height. The dotted curve is the fitted FFT spectrum.

from a periodic sinusoidal pattern was first introduced by Takeda *et al.* by a method known as fringe analysis using Fourier transform [13,14].

The WSI captures the pattern from a single point. As such, the entire phase shift values are related to a unique surface height; only one pixel is needed to acquire the pattern. By analyzing all the CCD pixels in an area detector imaging the surface individually, an areal topography can be obtained.

Since the wavenumber is scanned in a linear manner, the phase shift is changed linearly as well. Consequently the rate of change of the phase with wavenumber can be used to determine the optical path difference (and thus height), as stated in Eq. (5).

An example of an interference intensity pattern of one pixel obtained from the wavelength scanning process is shown in Fig. 2. The sinusoidal pattern in this figure has a slow-changing envelope function. This envelope is due in part to the changing width of the AOTF filter characteristic, where this change varies the light throughput across the tuned wavelength range. This systematic variation is eliminated by dividing the interference intensity pattern over the background intensity distribution along the scanned wavelength range. The compensated intensity pattern resulting from this operation is shown in Fig. 5(a).

Equation (2), which gives a mathematical expression of Fig. 5(a), can be presented in a more convenient alternate form as follows:

$$I_{xy}(i) = a_{xy}(i) + \frac{1}{2}b_{xy}e^{j\varphi(i)} - \frac{1}{2}b_{xy}e^{-j\varphi(i)}. \quad (10)$$

Equation (10) may be simplified by considering the following notation, $c = be^{j\phi(i)}/2$ and $c* = be^{-j\phi(i)}/2$, which lead to

$$I_{xy}(i) = a_{xy} + c_{xy} + c^*_{xy}. \quad (11)$$

An FFT is applied to Eq. (11) to find the spectrum of the interference pattern. In this paper the

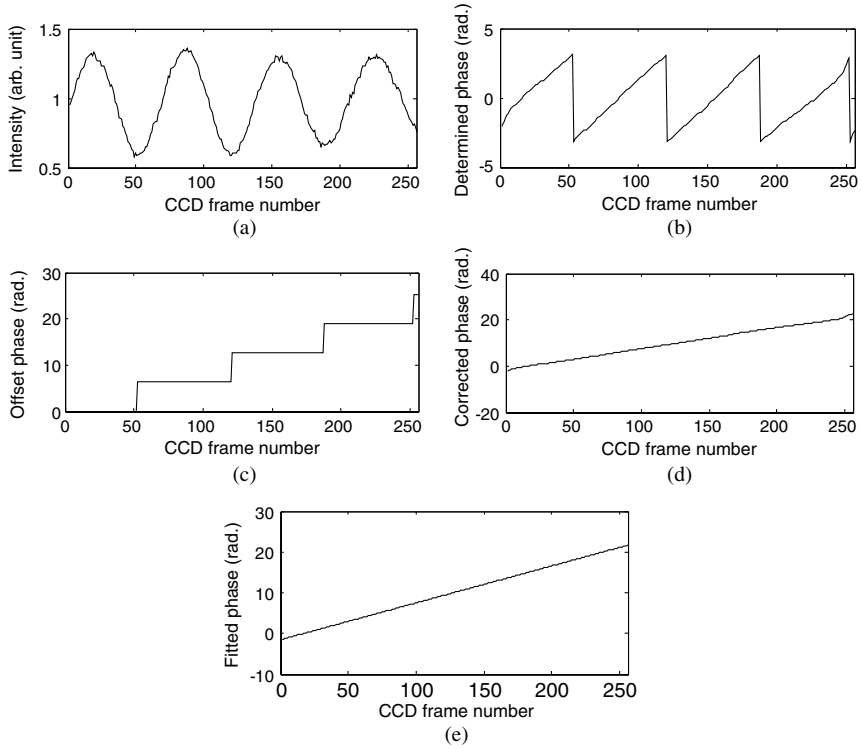

Fig. 5. Interference pattern analysis: (a) corrected interference pattern; (b) phase distribution with discontinuities; (c) 2π stair step function; (d) corrected phase distribution; and (e) fitted phase distribution.

spectrum of the FFT output contains three main terms, as stated in Eq. (12). The first term is a constant amplitude that relates to the light intensity in each interferometer arm; the second and third terms are related to phase shift that is achieved by scanning the wavelength of the white light. The purpose of FFT is to distinguish between the useful information that is represented by the phase change (i.e., c or c^* term) and the unwanted information of constant amplitude (i.e., A):

$$\mathrm{FFT}[I_{xy}] = A(f) + C(f - f_o) + C^*(f + f_o). \tag{12}$$

The f_o is a spatial frequency corresponding to the wavelength scanning and it is a function of the optical path difference. The unwanted spectrum A and C^* are filtered out and the inverse FFT is applied to the filtered pattern to reconstruct the c value in Eq. (11). Then, a natural logarithm is applied to separate the phase from the exponential term and the unwanted amplitude variation, as illustrated in Eq. (13):

$$\ln(b_{xy}e^{j\varphi(i)}) = \ln(b_{xy}) + j\varphi(i). \tag{13}$$

The phase is extracted from the imaginary part of Eq. (13) [see Fig. 5(b)]. Since the calculated phase is limited to a range of $-\pi$ to π, the phase distribution suffers from discontinuities. These discontinuities are corrected by adding a 2π staircase function to the phase distribution. Since the phase is shifted linearly, the staircase function adds 2π in an incremental manner, as shown in Figs. 5(c) and 5(d). The nonlinear deviations existing at the edges of the phase distribution are compensated for by using linear least square fitting approach [see Fig. 5(e)]. Finally the height, which is equal to half of the optical path difference, is calculated from the slope of phase distribution using Eq. (5).

The resolution at which the value of the phase shift may be determined, $\delta\varphi$, in this algorithm varies depending on the optical path difference. The following mathematical description is used to evaluate the measurement resolution. The entire phase shift $\Delta\varphi$ is assumed to be $2\pi(N + \varepsilon)$; the N is the number of fringe cycles within the interference pattern and ε symbol refers to the remaining fraction of the interference fringe pattern. As such, the phase resolution is

$$\delta\varphi = \frac{2\pi(N + \varepsilon)}{F}, \tag{14}$$

where F is the number of the captured frames, which equates to the total number of sampled points. The height resolution can be found by substituting Eq. (14) into Eq. (6), as given:

$$\delta h = \left(\frac{N + \varepsilon}{F}\right)\frac{\lambda_s}{2}. \tag{15}$$

This equation shows that the resolution can be improved by factor $(N + \varepsilon)/F$, compared to the simple FFT described in Section 3.A. For instance, if the surface height is located for example at 8.1 μm from the zero optical path difference, then $N + \varepsilon = 3.739$ and the resolution can be improved from 2.156 μm (using a simple FFT) to 0.031 μm for the measurement parameters.

However, because the resolution factor $(N + \varepsilon)/F$ is dependent on the surface height, each pixel has effectively a different resolution.

D. Localized Peaks of Interference Pattern Using Convolution: Algorithm D

The principle of fringe analysis using a convolution type method is based on determining the peaks positions of the interference pattern according to the scanned wavelength. This method was introduced by Schwider using a dispersive interferometer [15].

The surface height can be calculated by determining the number of peaks and their correspondence wavelength from the interference pattern. The position of the peaks can be found by convolving the interference pattern with a function having the following criteria:

$$f(x) = \begin{cases} -1 & 0 < x \le B \\ 1 & B < x \le 2B \end{cases}, \tag{16}$$

where x is the number of points of per convolved function. The 2B value is the width of the convolved function $f(x)$, which for optimum performance should be approximately 74% of the period width of the interference pattern, as proposed by Snyder in 1980 [16].

The convolution process produces a filtered first derivative of the sinusoidal interference pattern with no DC bias. Thus neither further filtration nor background intensity compensation is required to further manipulate the resulting signal. The obtained signal intersects the propagation axis at the original peaks positions as shown in Fig. 6. Thus, by monitoring the convolved signal for a sign change the positions of the peaks can be determined. When the signal value is changed from negative to positive value, a peak is present. However, these zero points are shifted from the original positions of the peaks by a magnitude equal to half of the $f(x)$ width (i.e., shifted by B value) due to the convolution integration effect. This effect has also reduced the number of samples by 2B value, as shown in the convolution axis of Fig. 6.

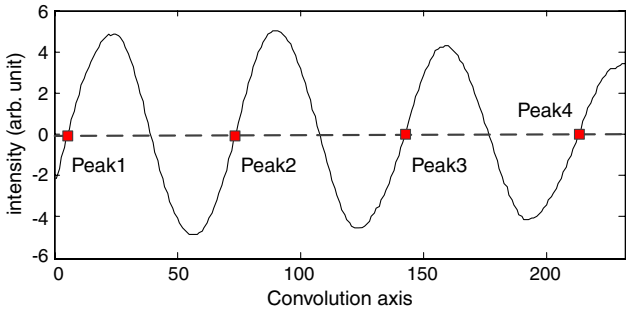

Fig. 6. (Color online) Convolution output.

Since the phase shift difference between two successive peaks is 2π, the surface height can be calculated by

$$h = \frac{N_{\mathrm{pk}} - 1}{2\left(\frac{1}{\lambda_m} - \frac{1}{\lambda_n}\right)}, \tag{17}$$

where λ_m and λ_n are the wavelengths of the first and last peaks, respectively, and N_{pk} is the number of peaks.

The following analysis can be used to evaluate the measurement resolution of this method. If the scanned wavelength range between λ_m and λ_n is $\Delta\lambda$, then Eq. (17) can be written as

$$h_1 = \frac{(N_{\mathrm{pk}} - 1)}{2} \frac{\lambda_m^2 + \lambda_m \Delta\lambda}{\Delta\lambda}. \tag{18}$$

The minimum height difference that can be resolved depends on the detection of the peak shift caused by a scanned wavelength step, $\delta\lambda$. The peak movement yields h_2 to be

$$h_2 = \frac{(N_{\mathrm{pk}} - 1)}{2} \frac{\lambda_m^2 + \lambda_m(\Delta\lambda - \delta\lambda)}{(\Delta\lambda - \delta\lambda)}. \tag{19}$$

By subtracting Eq. (18) from Eq. (19), the height resolution can be obtained as

$$\delta h = \frac{(N_{\mathrm{pk}} - 1)}{2} \frac{\lambda_m^2 2\delta\lambda}{\Delta\lambda(\Delta\lambda - \delta\lambda)}. \tag{20}$$

Equation (20) shows that the resolution depends both on the sampling frequency that is expressed by parameters $\delta\lambda$, and also the number of peaks. It is also dependent on the wavelength at which the first peak occurs, λ_m, as well as the wavelength range separation between the first and last peak, $\Delta\lambda$.

For example, the first and last peaks of the interference pattern in Fig. 2 are found to be located at 600.15 and 675.02 nm, respectively. Consequently, $\lambda_m = 600.15$ nm and $\Delta\lambda = 74.87$ nm. Since this interference pattern contains four peaks, the resolution is found to be 44.1 nm using Eq. (20).

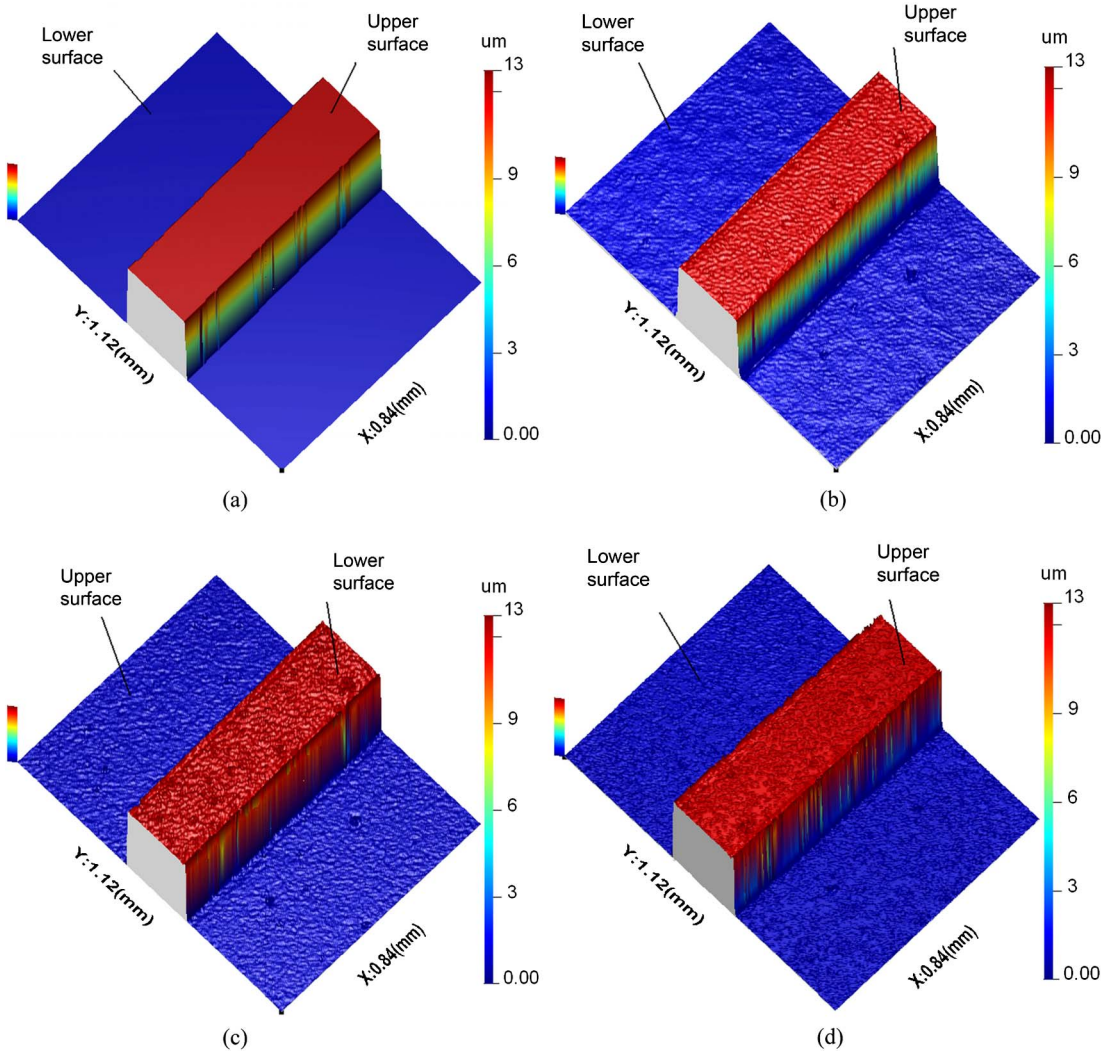

Fig. 7. (Color online) Areal measurement of 4.707 μm step-height standard sample using different algorithms (a) algorithm A; (b) algorithm B; (c) algorithm C; and (d) algorithm D.

Table 1. Measurement Results of a 4.707 μm Step-Height Standard Using the Four Different Algorithms[a]

Measured Parameters	Algorithm A (μm)	Algorithm B (μm)	Algorithm C (μm)	Algorithm D (μm)
Mean of LS height	8.663	8.358	8.150	8.161
Mean of US height	12.995	12.914	12.846	12.852
S_{5z} in LS	0	0.012	0.021	0.030
S_{5z} in US	0	0.028	0.030	0.042
Measured step height	4.332	4.556	4.696	4.691
Measurement error	0.375	0.151	0.011	0.016
Computation time (s)	11.63	100.14	32.56	19.43

[a]The LS and US are the lower and upper surfaces, respectively.

4. Experimental Results and Discussion

In order to confirm the performance of the algorithms discussed in the previous section, the WSI measurement system, as illustrated in Fig. 1, was used to measure two step-height standards having height values of 4.707 μm and 100 nm, respectively.

Figure 7 shows the four areal measurement evaluations of the 4.707 μm step-height sample using each of the previously described algorithms. The absolute displacement of the surfaces from the zero optical path difference and the sample step-height values are listed in Table 1. The step height is determined by finding the difference between the mean line value of the upper and lower sample surfaces. The maximum height of the topographic surface parameter S_{5z} is also given in this table. This parameter is found by calculating the average value of the absolute distance between five highest peaks and five lowest valleys within the surface. The algorithms are written with Matlab environment and processed by quad-core AMD Phenom II processor, the clock rate 2.5 GHz. The computation time is given in Table 1.

The obtained results show that the measurement error of step-height measurement has been improved from 0.375 to 0.011 nm. This variation in the measurement accuracy derives from the algorithm computation resolution. The areal measurement results contain surface roughness information, except the result obtained from algorithm A. The detected surface roughness information is due to the enhancement in measurement resolution. This enhancement also results in detection of low-level noise, such as environmental disturbances, which may cause additional measurement error. Table 1 shows that the S_{5z} values in the lower surface are less than the upper surface. This could be due to the variation in the measurement resolution for different heights, as illustrated in Eqs. (15) and (20).

The same analysis algorithms are used to evaluate the 100 nm step-height sample. The areal measurements and cross section profiles are shown in Figs. 8–10. Algorithm A was unable to recognize the step height while algorithm B can distinguish the step height of 100 nm but with error equal to 84 nm, as shown in Fig. 8(b). The two algorithms (C and D) found the step height to be equal to 100.8 and 102.3 nm, as shown in Figs. 9(b) and 10(b), respectively. The S_{5z} values on the two surfaces are the same for each algorithm. This is because the difference between the interference patterns of both surfaces is minimal; the fringe period sampling points of both patterns are almost the same. Therefore, maintaining the sampling of the interference patterns can sustain the resolution.

Table 1 shows that computing speed is influenced by the complexity of the algorithms. Clearly, the simple FFT is the fastest but results in the lowest measurement resolution. The fringe analysis using FFT shows that the speed is faster than the fitted FFT

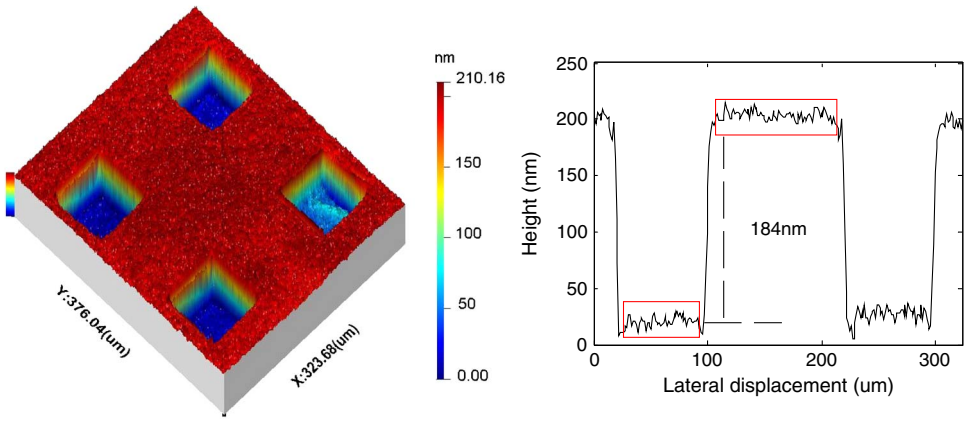

(a) (b)

Fig. 8. (Color online) Measurement of 100 nm standard step sample using algorithm B: (a) areal measurement and (b) cross section profile.

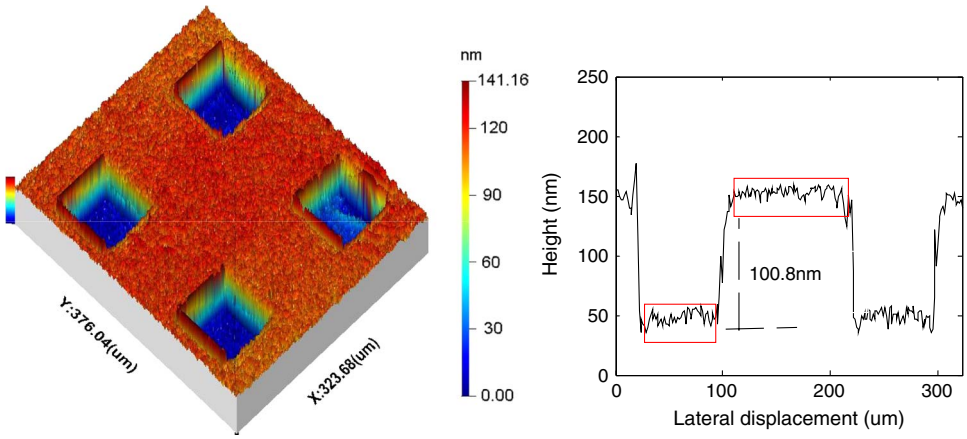

(a) (b)

Fig. 9. (Color online) Measurement of 100 nm standard step sample using algorithm C: (a) areal measurement and (b) cross section profile.

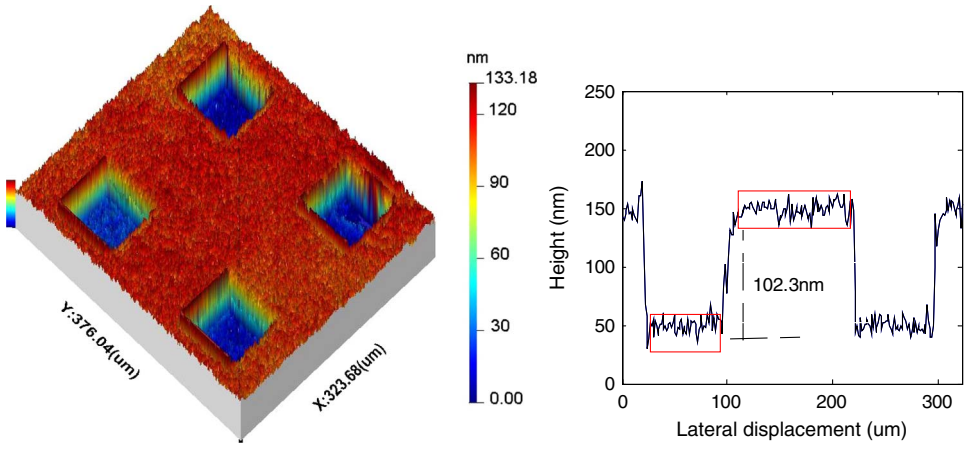

(a) (b)

Fig. 10. (Color online) Measurement of 100 nm standard step sample by using algorithm D: (a) areal measurement and (b) cross section profile.

and convolution methods. The computation time can be reduced to under 1 s for the datasets analyzed above by utilizing a many-core graphic processing unit using compute unified device architecture.

5. Conclusion

This paper shows that the accuracy of WSI measurement can be improved by considering a suitable algorithm to calculate the phase shift precisely. It is found that the height resolution is different for each algorithm. For instance, the δh in algorithm A is limited by $\lambda_s/2$. This resolution, on the other hand, is improved by factor $(N+\varepsilon)/F$ in algorithm C. According to this, the measurement accuracy is improved from micrometer to nanoscale, as illustrated in Table 1.

The measurement resolution depends on the optical path difference as well as the wavelength scanning range $\Delta\lambda$ and step $\delta\lambda$. It is found that the resolution is increased with surfaces close to the zero optical path difference. The S_{5z} value within surface profile is reduced by increasing the measurement resolution. This enhancement in the measurement resolution is due in part to increasing the sampling rate. However, if the measurement algorithm has a computing resolution below the surface S_{5z}, then no surface roughness information can be observed at any sampling rate.

The authors gratefully acknowledge the UK's Engineering and Physical Sciences Research Council (EPSRC) funding of the EPSRC Centre for Innovative Manufacturing in Advanced Metrology (Grant Ref.: EP/I033424/1). The author X. Jiang gratefully acknowledges the Royal Society under a Wolfson-Royal Society Research Merit Award and the European Research Council under its program ERC-2008-AdG 228117-Surfund. We would also like to thank Dr. Haydn Martin for fruitful discussion.

References

1. D. J. Whitehouse, *Handbook of Surface and Nanometrology* (Taylor & Francis, 2011).

2. N. Balsubramanian, "Optical system for surface topography measurement," U.S. patent 4,340,306 (4 February 1980).
3. S. Kuwamura and I. Yamaguchi, "Wavelength scanning profilometry for real-time surface shape measurement microscope," Appl. Opt. **36**, 4473–4482 (1997).
4. P. de Groot, X. C. deLega, J. Kramer, and M. Turzhitsky, "Determination of fringe order in white-light interference microscopy," Appl. Opt. **41**, 4571–4578 (2002).
5. H. Kikuta, K. Iwata, and R. Nagata, "Distance measurement by the wavelength shift of laser diode light," Appl. Opt. **25**, 2976–2980 (1986).
6. J. Thiel, T. Pfeifer, and M. Hartmann, "Interferometric measurement of absolute distances of up to 40 m," Measurement **16**, 1–6 (1995).
7. Y. Ishii, "Wavelength-tunable laser-diode interferometer," Opt. Rev. **6**, 273–283 (1999).
8. D. Xiaoli and S. Katuo, "High-accuracy absolute distance measurement by means of wavelength scanning heterodyne interferometry," Meas. Sci. Technol. **9**, 1031–1035 (1998).
9. A. Davila, J. M. Huntley, C. Pallikarakis, P. D. Ruiz, and J. M. Coupland, "Simultaneous wavenumber measurement and coherence detection using temporal phase unwrapping," Appl. Opt. **51**, 558–567 (2012).
10. X. Jiang, K. Wang, F. Gao, and H. Muhamedsalih, "Fast surface measurement using wavelength scanning interferometry with compensation of environmental noise," Appl. Opt. **49**, 2903–2909 (2010).
11. E. G. Bucher and J. W. Carnahan, "Characterization of an acousto-optic tunable filter and use in visible spectrophotometry," Appl. Spectrosc. **53**, 603–611 (1999).
12. A. Yamamoto, C. Kuo, K. Sunouchi, S. Wada, I. Yamaguchi, and H. Tashiro, "Surface shape by wavelength scanning interferometry using an electrically tuned Ti:sapphire laser," Opt. Rev. **8**, 59–63 (2001).
13. M. Takeda, H. Ina, and S. Kobayashi, "Fourier-transform method of fringe pattern analysis for computer based topography and interferometry," J. Opt. Soc. Am. **72**, 156–160 (1982).
14. M. Takeda and H. Yamamoto, "Fourier-transform speckle profilometry: three-dimensional shape measurements of diffuse objects with large heights steps and/or spatially isolated surfaces," Appl. Opt. **33**, 7829–7837 (1994).
15. J. Schwider and L. Zhou, "Dispersive interferometric profilometer," Opt. Lett. **19**, 995–997 (1994).
16. J. J. Snyder, "Algorithm for fast digital analysis of interference fringes," Appl. Opt. **19**, 1223–1225 (1980).